Thermohaline Circulation Below the Ross Ice Shelf: A Consequence of Tidally Induced Vertical Mixing and Basal Melting

Douglas Reed MacAyeal[1]

Geophysical Fluid Dynamics Program, Princeton University

The warmest water below parts of the Ross Ice Shelf resides in the lowest portion of the water column because of its high salinity. Vertical mixing caused by tidal stirring can thus induce ablation by lifting the warm but dense water into contact with the ice shelf. A numerical tidal simulation indicates that vertically well-mixed conditions predominate in the southeastern part of the sub-ice-shelf cavity where the water column thickness is small. Basal melting in this region is expected to be between 0.05 and 0.5 m/yr and will drive a thermohaline circulation having the following characteristics: high salinity shelf water (at −1.8°C), formed by winter sea-ice production in the open Ross Sea, flows along the seabed toward the tidal mixing fronts below the ice shelf; and meltwater (at −2.2°C), produced in the well-mixed region, flows out of the sub-ice-shelf cavity along the ice shelf bottom. Sensitivity of this ablation process to climatic change is expected to be small because high salinity shelf water is constrained to have the sea-surface freezing temperature.

INTRODUCTION

Substantial ablation from the Antarctic ice cap may result from ocean-heat transport into the cavity below the floating Ross Ice Shelf. Extrapolating from present ice-flow conditions, approximately 25% of the snow that falls on Antarctica will ultimately become part of the thick, integrated ice-shelf platform shown in Figure 1 [*Hughes*, 1975]. An estimate of the Ross Ice Shelf's mass budget based on available observations is presented in Table 1 and indicates that melting at the rate of 2×10^3 m/s is required to maintain a steady state. Present day melting at the top of the ice shelf is negligible; thus, if the mass budget is indeed stationary, the 5.8×10^5 km^2 base of the ice shelf must melt at an average rate of 0.11 m/yr. To accommodate this level of melting, the ocean must carry approximately 6×10^{11} W into the sub-ice-shelf cavity.

The inaccessibility of the region below the thick ice cover has greatly limited observations of the sub-ice-shelf environment from which to identify the prevailing circulation and basal melting patterns. The single available observation was taken through a bore hole at J9 (location shown in Figure 1). The temperature and salinity profiles of the J9 water column are shown in Figure 2 and are consistent with basal melting outside the immediate J9 area [*Jacobs et al.*, 1979; *Gilmour*, 1979; *Foster*, 1982]. Geochemical tracer measurements additionally indicate that the sub-ice-shelf waters are renewed by exchange with the open Ross Sea over a time scale of roughly 6 years [*Michel et al.*, 1979].

The warmest water below the ice shelf at J9 resides near the seabed because of its high salinity. The ice shelf base is isolated from this relatively warm water by an intervening layer of cold water exhibiting the geochemical traits of glacial meltwater (S. S. Jacobs and R. G. Fairbanks, unpublished manuscript, 1983). As a result of this temperature-depth profile, vertical heat transport through the water column, necessary to

support basal melting, requires mechanical energy to lift the warm but dense water into contact with the ice.

One likely source of mechanical energy below the ice shelf is the small-scale turbulence generated at the seabed and ice-shelf base by tidal currents. Ocean tides propagate freely through the ice-shelf-covered portion of the Ross Sea because the ice shelf is flexible over large horizontal scales [*Williams and Robinson*, 1981]. Sensitive gravimeters deployed across the ice-shelf surface by *Williams and Robinson* [1980] have indicated that the diurnal tidal amplitude exceeds a meter along the east coast of the ice-shelf-covered region. In view of the thick ice cover, turbulence generation by alternative means requiring air-sea contact is improbable. Tidal currents are thus identified as the most energetic stirring process throughout the sub-ice-shelf cavity.

This paper presents evidence based upon numerical tidal simulations [*MacAyeal*, 1983a] that suggests the following results: (1) tidal currents in select sub-ice-shelf regions sufficiently stir the water column to destroy stratification and thereby promote contact between the ice and the warm water near the seabed, and (2) a thermohaline circulation driven by meltwater production in the regions of strong vertical mixing may ventilate the deeper reaches of the sub-ice-shelf cavity.

HYDROGRAPHIC AND BATHYMETRIC SETTING

The proposed relationship between basal melting and strong tidal mixing is suggested by the observed Ross Sea hydrography and topography. A map of the depth in the open part of the Ross Sea and of the water column thickness below the ice shelf is presented in Figure 3. Broad areas where the water column thickness is less than 100 m are found in the southeastern section of the sub-ice-shelf region. Tidal currents tend to be strongest in regions where the water column is thin [*MacAyeal*, 1983a, b; *Williams*, 1976]; hence, tidal mixing is likely to be strongest in this part of the sub-ice-shelf cavity.

The seabed elevation in the region below the ice shelf is shown in Figure 4. A deep seabed channel extends toward the extreme southeastern corner of the sub-ice-shelf cavity and connects with the deepest part of the open Ross Sea near Ross Island. This channel provides a path that allows dense water formed in the open Ross Sea to drain into the region where strong tidal mixing may occur. Indeed, the dense water mass

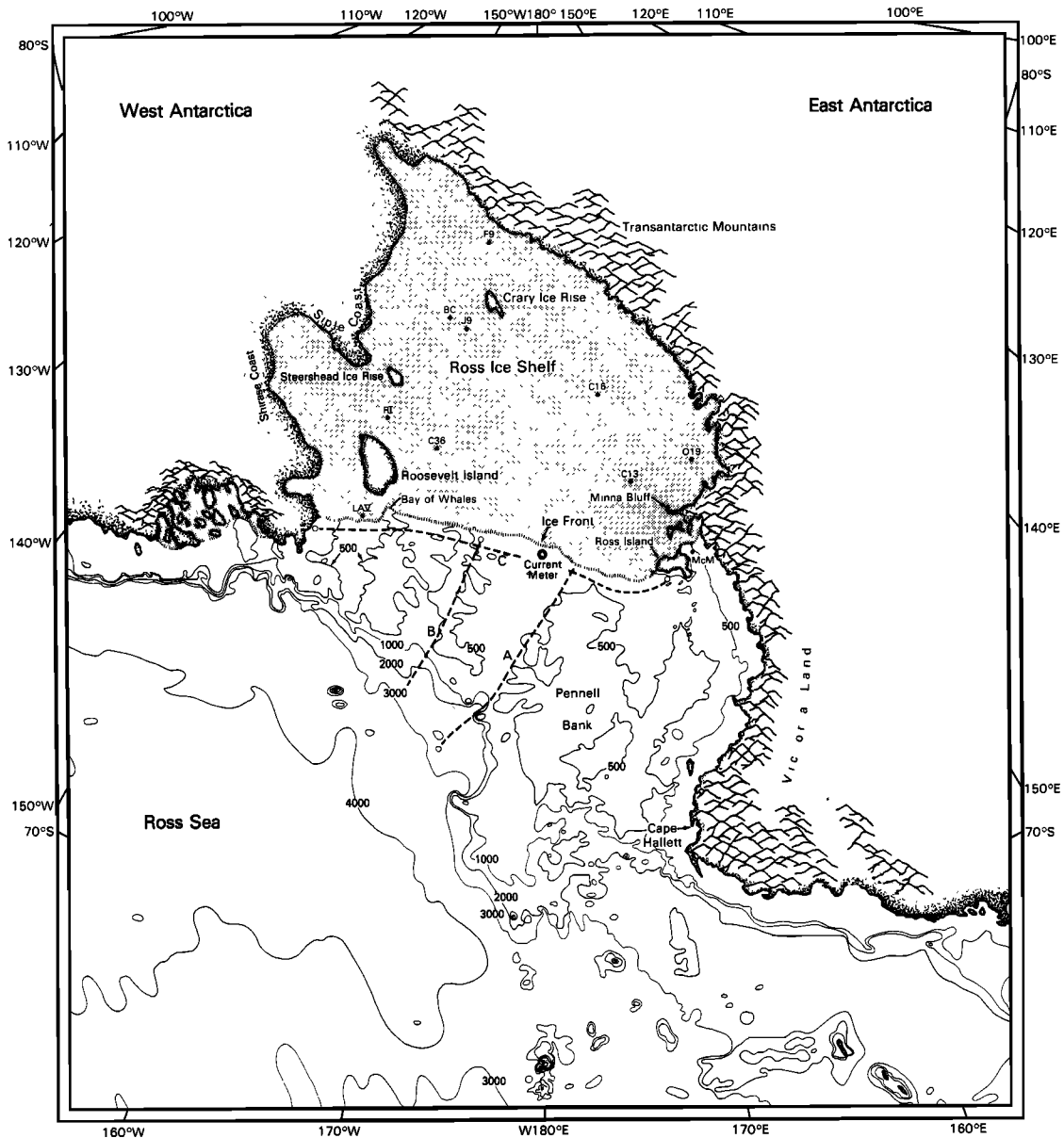[1] Now at Department of the Geophysical Sciences, The University of Chicago.

Fig. 1. Large floating ice shelves at the margins of the west Antarctic ice sheet extend seaward from where the ice floats free of the sea bed. The Ross Ice Shelf, shown above as the shaded area, occupies the southern half of the Ross Sea. It ranges in thickness from 1100 to 100 m, covers an area of 5.8×10^{11} m^2, and flows toward the open ocean at a rate of up to 1100 m/yr. Air-sea contact is prohibited within the sub-ice-shelf cavity; hence, tidal currents are the dominant cause of vertical mixing in the water column. This paper presents the results of numerical tidal simulations that indicate tidal front formation and related thermohaline circulation below the ice shelf.

known as high salinity shelf water (HSSW) does comprise the lower portion of the water column at J9 and is thus expected to exist below most parts of the ice shelf where the seabed elevation is sufficiently depressed [Jacobs et al., 1970]. The temperature θ of HSSW varies little from the sea-surface freezing point, and its salinity S is higher than 34.75 ‰. As shown

TABLE 1. An Estimated Mass Budget of the Ross Ice Shelf Assuming Steady State

	Parameter, m³/s
Ice stream and glacier inflow	3×10^3
Snow accumulation	3×10^3
Iceberg calving	-4×10^3
Basal melting	-2×10^3

in Figure 5, HSSW occupies the seabed depression north of Ross Island and is partially blocked from draining off the continental shelf by the Pennell Bank.

Gill [1973] and Killworth [1974, 1977] hypothesized that salt released by freezing within near-shore sea ice leads creates HSSW at a rate exceeding 1.0×10^6 m³/s in the Ross Sea. The nearly uniform temperature of HSSW, being tied to the sea surface freezing point, is 0.2°C to 0.5°C higher than the freezing point of the ice shelf base because of the greater hydrostatic pressure below the ice [Gill, 1983, p. 602]. Gill [1973] thus proposed that HSSW would induce basal ablation wherever strong stratification did not prevent its contact with the ice shelf base. Possible erosion of stratification by tidal currents was considered; but Gill [1973], at the time of his study, lacked sufficiently accurate measurements of sub-ice-shelf tides and bathymetry to investigate this issue further. The study
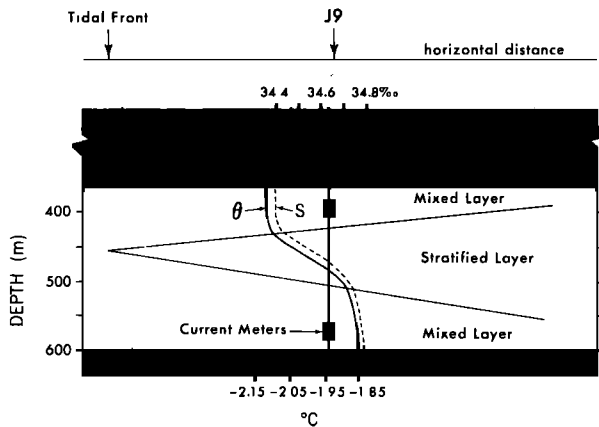
Fig. 2. The observed temperature (θ) and salinity (S) profiles below the ice shelf at the J9 drill camp (location shown in Figure 1) are displayed along with the hydrographic structure expected to result from the proposed tidal front southeast of J9 [Fearnhead, 1975]. The θ and S data were obtained from Jacobs et al. [1979] and Gilmour [1979]. The vertical shear of the time-average current observed by Jacobs at J9 [Jacobs and Haines, 1982] indicates that the isopycnal surfaces are inclined downward toward the tidal front.

presented in this paper adapts Gill's [1973] hypothesis to the region below the Ross Ice Shelf by employing more recent observations and a numerical simulation of the tidal regime.

PROPOSED CIRCULATION OF HSSW

The distribution of HSSW in the sub-ice-shelf cavity may be estimated by using the observed hydrography in the open Ross Sea and below the ice at J9. The upper limit of HSSW at J9 is approximately 500 m below sea level and is consistent with the upper limit found throughout much of the open Ross Sea [Jacobs et al., 1979; Jacobs and Haines, 1982]. Assuming that HSSW fills the seabed depression below the ice shelf up to the 500 m level, HSSW will exist in most parts of the sub-ice-shelf cavity except where the seabed is higher than 500 m below sea level. These zones where HSSW is excluded are represented by the unshaded parts of the map in Figure 4.

The ice shelf draft, shown in Figure 6, is less than 500 m except in the extreme southeastern corner of the Ross Sea. HSSW will thus outcrop onto the ice shelf base over a relatively small area. Even in these regions of possible outcrop, contact between HSSW and the ice would quickly be suppressed because, as Gill [1973] pointed out, meltwater would form a protective film along the ice shelf base and diminish further heat transfer from below. Protective films and other water layers intervening between HSSW and the ice are eroded, however, wherever tidal currents induce strong turbulence.

To estimate where vigorous tidal mixing will lift HSSW into contact with the ice, the sub-ice-shelf cavity is partitioned into the following two sets: (1) the areas where the water column thickness is less than 100 m (where tidal currents will be strongest) and (2) the areas where HSSW is not excluded by high seabed elevations (where there is a heat source). This intersection is displayed schematically in Figure 4 and occurs primarily along the seabed ridge extending between the Siple Coast and Crary Ice Rise. Basal melting in this area would counteract an ice shelf thickening tendancy determined from the observed ice movement and snow accumulation rate and would imply that the ice shelf mass balance in this area is in steady state [Thomas and Bentley, 1978].

If significant basal melting occurs in the intersection defined above, then buoyancy production associated with dilution by meltwater will tend to drive a thermohaline circulation having the following characteristics: (1) warm HSSW is drawn into the sub-ice-shelf cavity along the seabed from its source in the open Ross Sea, (2) the relatively high temperature of HSSW is preserved until the HSSW encounters strong vertical mixing along the Siple Coast (heat diffused out of this water mass into the fresher water above is assumed to be small), and (3) contact between inflowing HSSW and the ice in the well-mixed region extracts the available heat and produces a meltwater-laden offspring water mass that exits the sub-ice-shelf cavity along the sloping ice shelf bottom. Eventually, the outflowing meltwater will reach a level of neutral buoyancy and will intrude between the inflowing HSSW and the fresh surface waters of the open Ross Sea. It is therefore reasonable to expect meltwater off the ice front at intermediate depths.

DEEP ICE SHELF WATER

Glacial meltwater can be identified by its temperature, salinity, and geochemical composition. Glacial ice derived from snowfall has zero salinity and an extremely low Oxygen 18 to Oxygen 16 isotopic ratio (δ) relative to standard seawater; thus dilution of HSSW by basal melting predictably reduces its temperature, salinity, and δ [Weiss et al., 1979]. Perhaps the most distinctive feature of meltwater produced below an ice shelf, however, is that its temperature is below that attainable at the sea surface. This temperature results from the depressed freezing point that accompanies the high hydrostatic pressure at the ice shelf base [Lusquinos, 1963; Gill, 1982, p. 602].

S. S. Jacobs and R. G. Fairbanks (unpublished manuscript, 1983) have conducted a careful water mass census based on observed temperature, salinity, and δ and have identified sev-
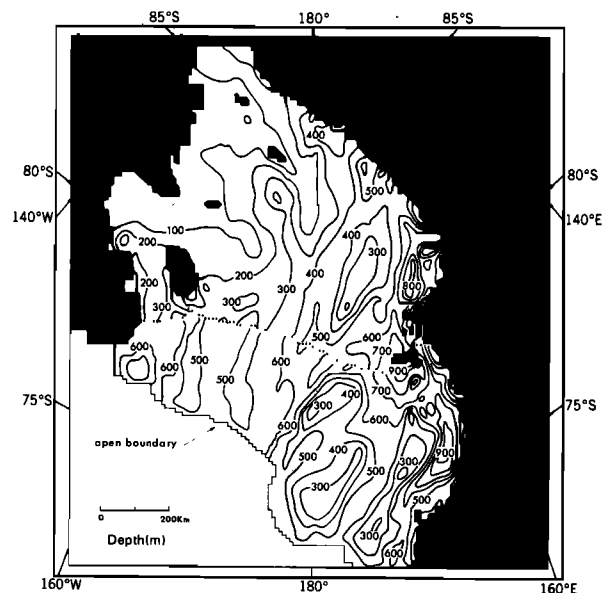

Fig. 3. Depth in the open portion of the Ross Sea is obtained from Hayes and Davey [1974]. The water depth south of the ice front (dotted line) is defined as the thickness of the water column alone and is obtained from Greischar and Bentley [1980]. The tidal currents are strongest in the portion of the sub-ice-shelf cavity where the water column thickness is less than 100 m. Vertically well-mixed conditions are thus expected in these shallow regions along the Siple Coast.
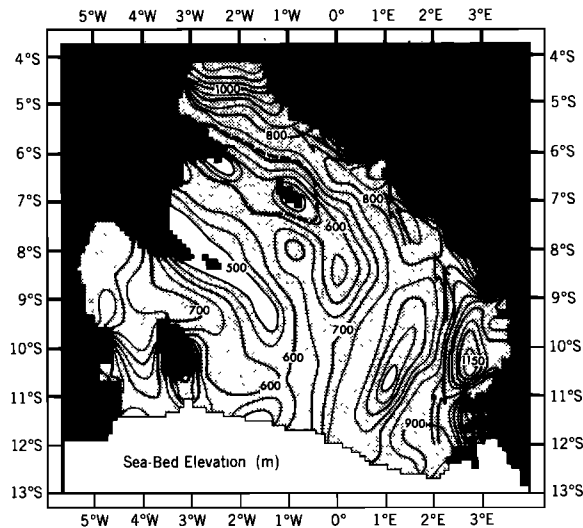
Fig. 4. The seabed elevation in the sub-ice-shelf cavity is obtained by adding the observed ice shelf draft [Bentley et al., 1979] to the observed water column thickness presented in Figure 3. Assuming that the 500 m upper limit of HSSW in the water column at J9 applies everywhere, HSSW will penetrate into most regions of the sub-ice-shelf cavity (indicated by shading). Strong tidally induced vertical mixing is expected to promote efficient heat transfer between HSSW and the ice shelf base above the seabed ridge extending between the Siple Coast and Crary Ice Rise. Basal melting is thus expected to be strongest in this part of the sub-ice-shelf cavity. Tidal fronts expected to surround the zone of strong vertical mixing and basal ablation are indicated schematically by the broken lines. The proposed thermohaline circulation that carries heat into the basal-melting region is indicated by the arrows drawn in the seabed channel running along the west coast. HSSW is expected to flow down this channel in response to outflowing meltwater produced where HSSW finally crosses the tidal fronts. False latitudes and longitudes at the outer margins of the above map are constructed by placing the false north pole at the intersection of the equator and prime meridian. This false coordinate system is the convention adopted for presentation of Ross Ice Shelf data [Bentley et al., 1979].

eral water masses displaying the characteristic signature of ice shelf meltwater. One particular water mass known as deep ice shelf water (DISW) displays the characteristics derived from HSSW ($\theta \le -2.0°C$, $S \ge 34.7$ ‰, $\delta \le -0.5$ ‰) and is observed off the ice front at depths in excess of approximately 400 m (S. S. Jacobs and R. G. Fairbanks, unpublished manuscript, 1983).

Hydrographic observations along the ice front provide evidence that DISW may indeed be formed as part of a thermohaline circulation driven by melting along the Siple Coast. As shown in Figures 7 and 8, DISW is observed protruding from the sub-ice-shelf cavity along the mid-section of the ice front and at depths in excess of 400 m [Jacobs et al., 1970; Jacobs et al., 1979]. Buoyancy considerations suggest that meltwater will rise to a level shallower than that where it originated. The zone of basal melting where DISW is derived is thus likely to correspond with the region where the ice shelf draft exceeds 400 m. As indicated by shaded parts of Figure 6, 400 m is exceeded primarily in the region along the Siple Coast where the water column is likely to be intensely mixed. Meltwater produced below thinner portions of the ice shelf will emerge from below the ice at depths substantially shallower than 400 m. S. S. Jacobs and R. G. Fairbanks (unpublished manuscript, 1983) report that such meltwater is found off the ice front at approximately 200 m depth and is hydrographically distinct from the DISW below.

Observed hydrographic properties off the Filchner and

Ronne ice shelves in the Weddell Sea show traits similar to those of the Ross Sea described above. As shown in Figure 8, temperatures less than $-2°C$ are observed at depths between 300 and 1100 m along the Filchner ice front [Carmack and Foster, 1975; Gammelsrod and Slotsvik, 1981]. Considering the great depth of $-2°C$ outflow found along the Filchner ice front, ice shelf meltwater production in the Weddell Sea may also occur where the ice shelves shoal and where the Weddell Sea tidal currents may be strong.

Simulated Tidal Energy Budget

The thick ice cover prevents air-sea contact; thus the tidal current is the principal source of small-scale turbulence in the southern Ross Sea. The rate at which energy is transferred from the large-scale tidal flow to the small-scale turbulence is parameterized by a quadratic drag law: $k|u|u \cdot u$ [Ramming and Kowalik, 1980, p. 17]. In this expression, u is the depth-averaged tidal flow and k is a nondimensional parameter approximately equal to 2.5×10^{-3} in ice-free water and 5.0×10^{-3} below the ice shelf (to account for the additional friction at the ice shelf base). To provide an energy transfer to turbulence, the tide must establish a mechanical energy flux that is convergent where $k|u|u \cdot u$ is large. The equation expressing this energy continuity is written [Ramming and Kowalik, 1980, p. 194]:

$$0 = -\nabla \cdot \langle u(g\rho D\eta + \rho D \tfrac{1}{2}|u|^2) \rangle - \langle \rho k|u|u \cdot u \rangle \qquad (1)$$

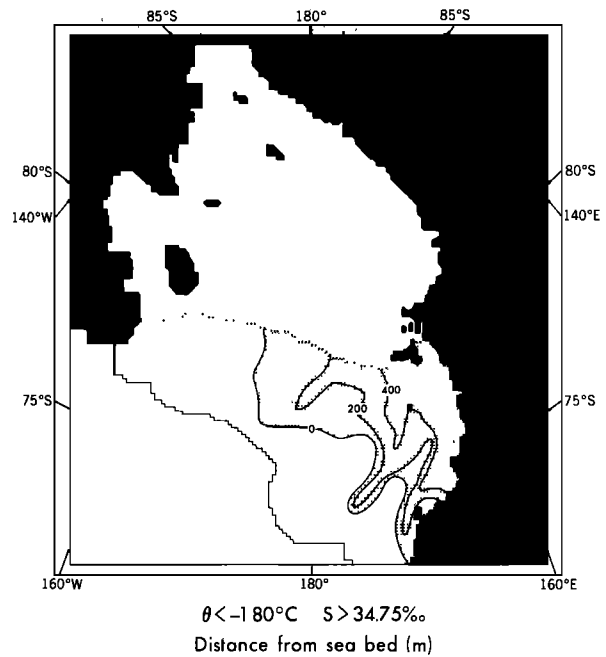$\theta < -1\,80°C \qquad S > 34.75‰$

Distance from sea bed (m)

Fig. 5. High salinity shelf water (HSSW) is the most dense water mass found on the continental shelves of the Ross and Weddell seas [Jacobs et al., 1970; Gill, 1973]. In this diagram, the observed areal disposition of HSSW in the Ross Sea is displayed by shading [reproduced from Jacobs et al., 1970]. The vertical distance between the upper limits of this water mass and the seabed is contoured in meters. This water mass forms by surface water densification and convection associated with winter sea ice growth [Gill, 1973]. Its temperature is thus constrained to be the sea surface freezing point and is several tenths of a degree (C) above the in situ melting point at the base of the Ross Ice Shelf. Observations through the J9 bore hole indicate that HSSW was prevalent near the seabed within the sub-ice-shelf cavity but was not in contact with the ice shelf base. It is argued in this study that strong vertical mixing induced by tidal currents along the shallow Siple Coast lifts the HSSW into contact with the ice shelf and thereby catalyzes basal melting.
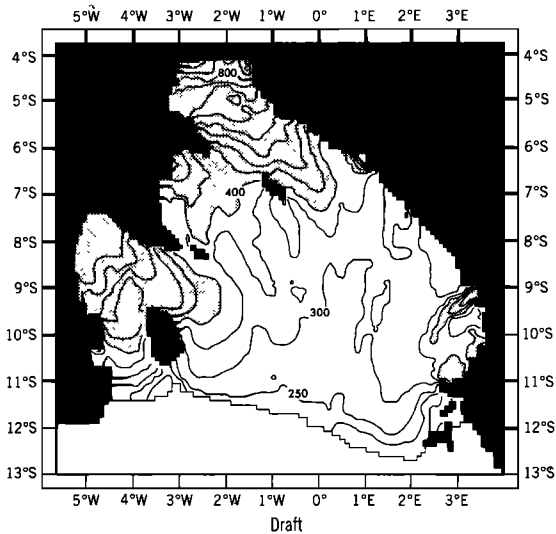
Fig. 6. The ice shelf draft observed by *Bentley et al.* [1979] is contoured in meters, and regions exceeding 400 m are denoted by shading. Meltwater is observed off the ice front at depths predominantly greater than 400 m. Buoyancy considerations suggest that this meltwater must therefore originate in the shaded regions of the above diagram. The zones of strong vertical mixing also correspond with the shaded regions; hence, the depth of the observed meltwater off the ice front provides consequential evidence in support of the proposed relationship between basal melting and tidally induced mixing.

where η is the displacement of the sea surface (or ice shelf base) from the level of equilibrium, D is the water column thickness (Figure 3), ρ is the seawater density (1027 kg/m³), g is the gravitational acceleration (9.81 m/s²), $\langle\ \rangle$ is the time-averaging operator defined by,

$$\langle\ \rangle = T^{-1} \int_0^T dt \qquad (2)$$

and T is a time period over which tidal oscillations average to zero.

The first term on the right-hand side of equation (1) represents the time-averaged energy-flux convergence and is primarily associated with the work done by tidal currents against pressure, $u\rho gD\eta$. Figure 9 displays the tidal energy flux into the sub-ice-shelf cavity given by the numerical simulations discussed in a companion paper [*MacAyeal*, 1983a]. Figure 10 presents a comparison between the simulated and the observed fluxes at the location of the ice-front current-meter mooring shown in Figure 1 [*Jacobs and Haines*, 1982].

The tidal energy dissipation rate $\langle k|u|u \cdot u\rangle$ is displayed in Figure 11. This rate exceeds 0.02 W/m² at three locations: the seabed ridges extending out from the Siple Coast, the ice front section northwest of Roosevelt Island, and along the continental shelf margin. High energy dissipation northwest of Roosevelt Island is due to diurnal period topographic Rossby waves that propagate along the ice front [*Longuet-Higgins*, 1968]. Observational evidence in support of high energy dissipation at this site is provided by the diatom abundances observed in the seafloor sediments. *Truesdale and Kellogg* [1979] report that an assemblage of light and fragile diatom skeletons, abundant elsewhere in the Ross Sea, is missing from this section of the ice front. They interpret this scarcity as a result of selective winnowing by strong bottom currents. *Pingree and Maddock* [1977] and *Pingree* [1980] found a similar correlation between coarse bottom sediments and high tidal energy dissipation in the English Channel.

The simulated rate of tidal energy dissipation within the entire sub-ice-shelf region, disregarding possible losses by nonelastic ice shelf flexure, is 3.5×10^9 W. This rate accounts for approximately 0.2% of the estimated 1.5×10^{12} W loss due to seabed friction over the entire continental shelf area of the earth [*Miller*, 1966]. Viewed in relation to tidal energy dissipation levels in other parts of the world ocean, the value found here is approximately 7% of the dissipation rate in the Arctic Ocean (as estimated by *Kowalik and Untersteiner* [1978]), and 10% of that in the Gulf of Maine excluding the Bay of Fundy (as estimated by *Greenberg* [1979]). Much of the tidal energy dissipation in the Ross Sea results from topographic Rossby wave propagation along such features as the ice front and the seabed ridges near the Siple Coast [*MacAyeal*, 1983a]. This aspect of the Ross Sea dissipation is similar to that occurrring along the margins of the Barents Sea [*Huthnance*, 1981].

SUB-ICE SHELF TIDAL FRONTS

A tidal front is the hydrographic transition between a vertically well-mixed and a stratified region. A given water column has less gravitational potential energy when it is stratified than when it is vertically homogeneous; thus tidal front positions may be predicted by comparing the local rate of tidal energy dissipation to the local rate at which gravitational potential energy is removed from the water column by buoyancy fluxes [*Simpson*, 1971; *Fearnhead*, 1975; *Simpson and Hunter*, 1974]. Wherever the dissipation rate is insufficient to increase the gravitational potential energy to the value attained by a vertically homogeneous density profile, the water column will remain stratified. Below the ice shelf, stratification is maintained by local melting, by horizontal advection of meltwater along the ice-shelf base, and by horizontal advection of HSSW along the seabed.

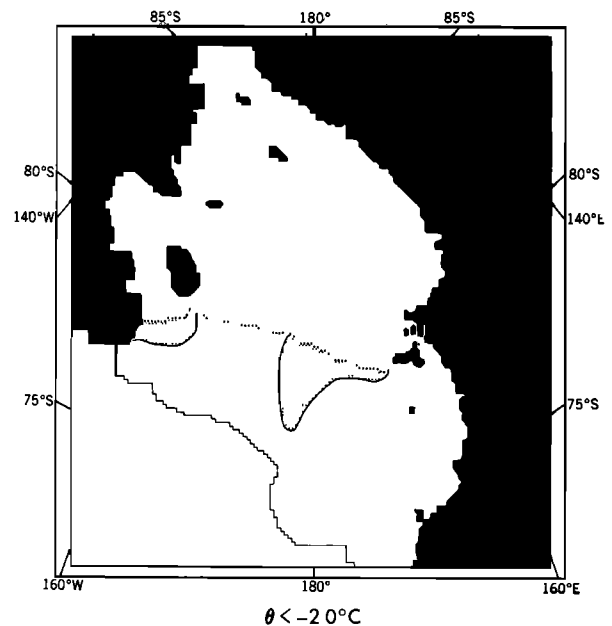Considerable success has been achieved in predicting the

$\theta < -20°C$

Fig. 7. Deep ice shelf water (DISW) is a water mass observed at mid-depth that has a temperature less than the sea surface freezing point (at the same salinity). This supercooled temperature can only be attained at pressures associated with the draft of the ice shelf base. The observed areal disposition of DISW is indicated by shading [reproduced from *Jacobs et al.*, 1970]. It is argued in this study that DISW is formed by melting in the tidally well-mixed parts of the sub-ice-shelf cavity.
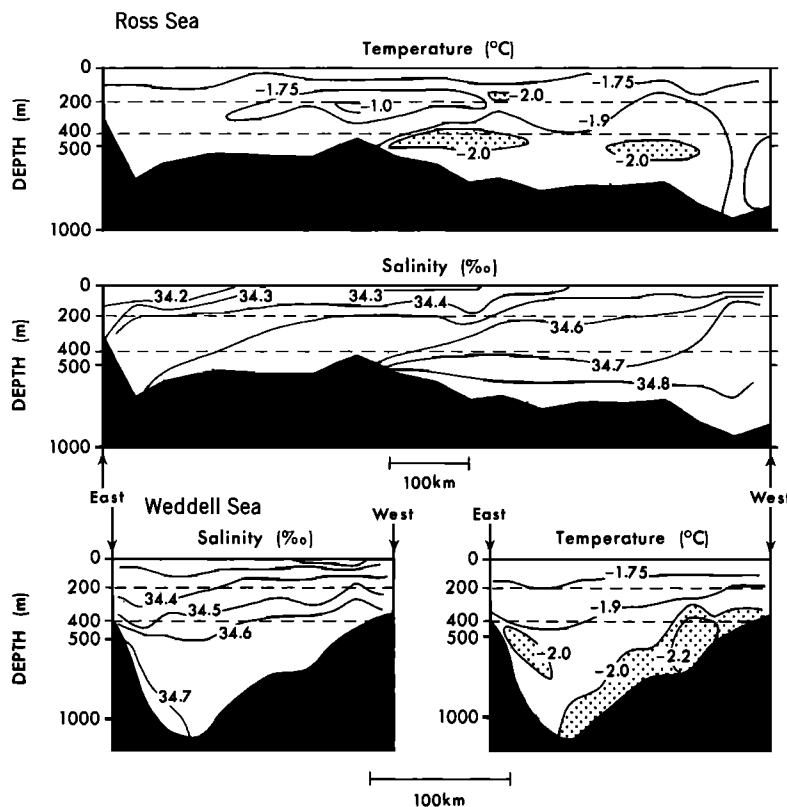
Fig. 8. Observed temperature and salinity are plotted on cross sections of the Ross and Weddell seas that lie parallel to the ice fronts of the Ross and Filchner ice shelves, respectively (Ross Sea observations reproduced from *Jacobs et al.*, [1979]; Weddell Sea observations reproduced from *Carmack and Foster* [1975]). The cross section of the Ross Sea is labeled C in Figure 1. In both the Ross and Weddell seas, water flowing out from below the ice shelves has temperature less than −2°C (indicated by stippling). The depth of this observed outflow generally exceeds 400 m and indicates that sites of basal melting where this water mass originates must correspond with ice shelf draft greater than 400 m. In the Ross Sea, the regions having such large draft also correspond with the tidally well-mixed regions indicated in Figure 6. Meltwater observed flowing out from below the Filchner Ice Shelf in the Weddell Sea at depths greater than 400 m suggests that tidally induced vertical mixing may excite a thermohaline circulation similar to that proposed below the Ross Ice Shelf.

locations of tidal fronts in the shallow seas surrounding northwestern Europe from information provided by numerical tidal simulations [*Pingree and Griffiths*, 1978; *Pingree*, 1980]. The empirical techniques established in these studies are used here to determine potential tidal front locations below the Ross Ice Shelf.

The tidal energy budget given by the numerical simulation provides half of the information needed to accomplish this prediction. The basal-melting pattern comprises the other half but is largely unknown. It is thus not possible to calculate the tidal front locations directly.

The indirect approach used here is summarized as follows: (1) calculate the minimum local melting rate required to maintain stratification against the known tidal energy dissipation rate provided by the numerical simulation and (2) compare this minimum melt rate with the probable range of actual basal melting. Some portions of the sub-ice-shelf cavity are found to require a far higher basal melting rate than that given by even the most liberal estimate of actual conditions. These regions are predicted to be vertically well mixed, and tidal fronts are expected to lie somewhere just outside these regions.

The minimum local basal melting rate required to maintain stratification F_m is calculated by using the following formula:

$$F_m = \alpha\rho\langle k|u|u \cdot u\rangle/(1/2\rho\beta gSD) \qquad (3)$$

where $\beta = 1/\rho \ (\partial\rho/\partial S) = 0.8 \times 10^{-3} \ (\text{‰})^{-1}$ [*Gill*, 1982, p. 599], $S = 34.75$ ‰ is the salinity of HSSW, and $\alpha = 0.01$ is an efficiency factor representing the fraction of the total tidal energy dissipation ultimately expended in the erosion of stratification [*Fearnhead*, 1975]. The value of α used in this study is derived from previous studies that estimate α on the basis of observed tidal front positions [*Fearnhead*, 1975; *Schumacher et al.*, 1979]. These estimates range between 0.01 and 0.02, so the value adopted here represents a conservative estimate.

The numerator on the right-hand side of equation (3) represents the energy input per unit area available for mixing. The denominator represents the work required to entrain surface meltwater input of unit flux (m/s) into an otherwise well mixed but salty water column of depth D [*Fearnhead*, 1975]. The minor effect of temperature on the density of saltwater near the freezing point is disregarded in equation (3).

Figure 12 displays the contours of F_m plotted throughout the Ross Sea. North of the ice front, the contours are displayed only for comparison, and are not intended to be meaningful since air-sea contact will introduce additional buoyancy fluxes not of interest in this study.

As stated previously, basal melting conditions are largely unknown; hence, the values of F_m in Figure 12 that exceed the actual melting rate F cannot be identified in a straightforward manner. Reasonable estimates of F can be attained by a number of means, all of which yield a consistent result. A
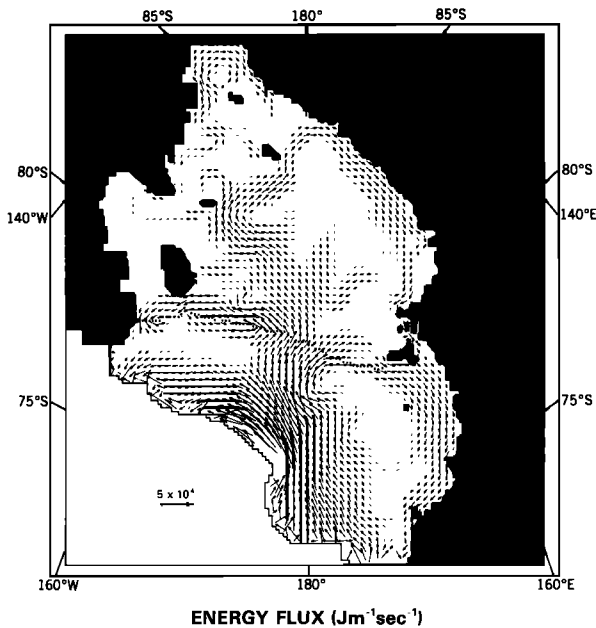
ENERGY FLUX (Jm⁻¹sec⁻¹)

Fig. 9. The time-average tidal energy flux vectors are drawn at every other grid point of the numerical domain. The majority of the energy flux into the sub-ice-shelf cavity crosses the ice front where the water depth is large.

simple geochemical box model, for example, can be constructed by assuming that HSSW is the inflow, DISW is the outflow, and that the vertically well-mixed regions where melting occurs comprise approximately 10% of the sub-ice-shelf cavity (5.8×10^4 km²) [*MacAyeal*, 1983b]. A computation of the heat, salt, and mass budgets of this box yields a melting rate of approximately 0.05 ± 0.02 m/yr.

An alternative method for estimating the actual basal melting rate is based on the residence time of HSSW below the ice shelf, determined from radioactive tracer concentrations observed at J9 [*Michel et al.*, 1979]. This residence time implies that a volume of approximately $1.0 \pm 0.5 \times 10^{14}$ m³ of HSSW circulates through the sub-ice-shelf cavity every 6 years. Assuming that this volume loses all of its available heat to basal melting and to upward heat flux through the ice shelf (assumed to require the heat equivalent of 0.03 m/yr freezing) [*Clough and Hansen*, 1979], a meltwater flux of $2.0 \pm 1.0 \times 10^3$ m³/s can be expected. The net basal melting rate in the well-mixed region (comprising 10% of the total sub-ice-shelf area) is approximately 0.50 ± 0.25 m/yr.

Both of the basal-melting estimates derived above suggest that melting does not exceed approximately 0.50 m/yr in parts of the sub-ice-shelf cavity that are remote from other sources of ocean heat besides that of HSSW. Near the ice front, however, basal melting is expected to be higher because of a southward flow of relatively warm and fresh water observed above HSSW in the open Ross Sea [*Jacobs et al.*, 1979]. This ice-front zone does not correspond with the major areas of strong tidal mixing (except along the ice front just northwest of Roosevelt Island), so is not of further concern in this study.

Areas where vertically well-mixed conditions are expected on the basis of a 0.05 m/yr basal-melting criterion are shaded in Figure 12. This criterion is a conservative estimate of the present basal melting conditions; thus, the shaded area of Figure 12 represents the maximum estimated extent of well-mixed conditions. The minimum estimated extent, based on a 0.5 m/yr criterion, is approximately half the area of the

shaded region in Figure 12 and would be enclosed within a contour lying halfway between the 0.1 m/yr and the 1.0 m/yr contours of Figure 12. The boundaries between the shaded and the unshaded regions define the approximate locations of tidal fronts. The uncertainty level of these boundaries is expected to be approximately 50 km and is estimated on the basis of the probable range of present basal melting and the uncertainty of the parameters α and k.

Thermohaline Circulation Scenario

As stated previously, meltwater production in the zones of strong tidal mixing may drive a thermohaline circulation in the sub-ice-shelf cavity. The vigor of this circulation can be estimated by considering its mechanical energy budget. As with other forms of buoyancy-driven circulation, a balance is achieved between the release of gravitational potential energy and the energy expended as work against friction. For simplicity in this preliminary analysis, the following effects are disregarded: other forms of energy dissipation besides friction at the seabed and ice-shelf base, the exchange of heat and salt between the inflow and outflow by diffusion outside the well-mixed Siple Coast, and the vertical heat flux through the ice shelf is disregarded. An idealized channel closed at one end represents the sub-ice-shelf cavity in this analysis. Variation of currents across this channel as a result of the earth's rotation are additiondally disregarded. The rate of gravitational potential energy release B and the energy dissipation rate E for the thermohaline convection are approximated by

$$B = g\Delta D\ \Delta\rho\ u_c\ Wh \tag{4}$$

and

$$E = \rho\ L\ W\ \langle k|u|\rangle\ u_c^2 \tag{5}$$

where u_c is the horizontal velocity (positive for inflow and negative for outflow), ΔD is the vertical separation between the cores of the inflow and outflow at the ice front (taken from observations), $\Delta\rho$ is the density difference between the inflow and outflow, h is the thickness of the inflowing and
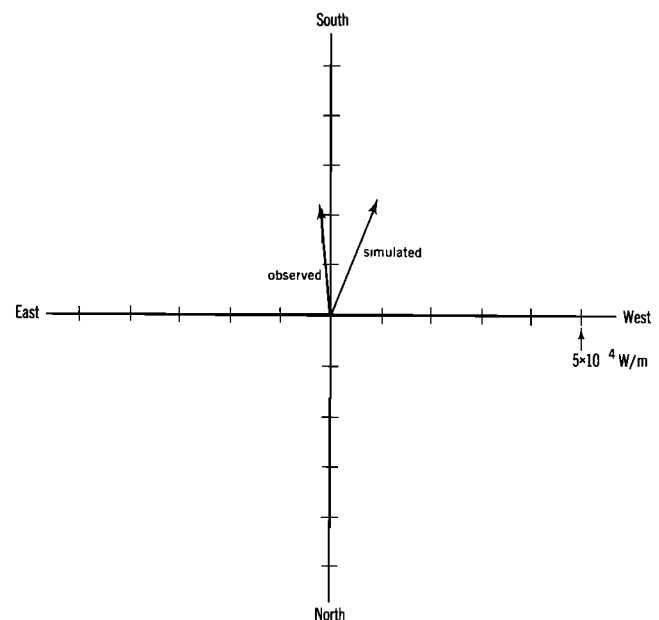

Fig. 10. The simulated and observed energy-flux vectors at the location labeled "current meter" in Figure 1 are compared.
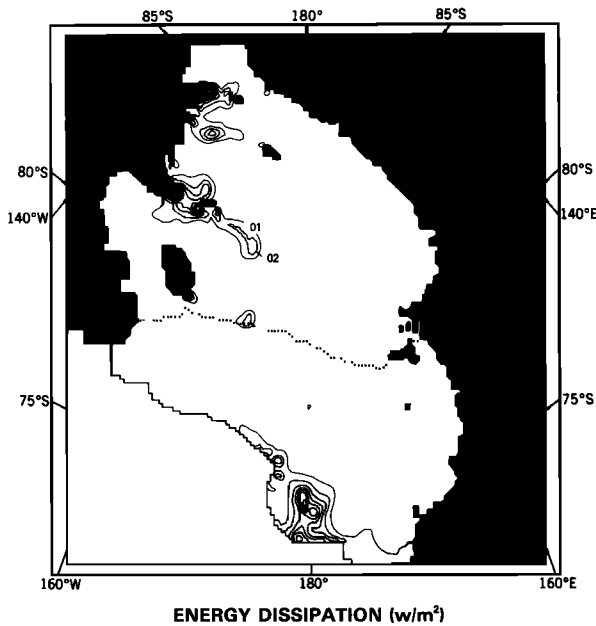
ENERGY DISSIPATION (w/m²)

Fig. 11. There are three principal sites of tidal energy dissipation: (1) along the seabed ridges extending away from the Siple Coast, (2) at a spot along the ice front northwest of Roosevelt Island, and (3) along the northern margin of the Pennell Bank. Site 1 results from high tidal amplitudes and shallow depths that intensify the tidal currents. Site 2 results from diurnal period topographic Rossby waves excited along this particular segment of the ice front. Site 3 results from large semidiurnal tidal currents along the open boundary. The total simulated energy dissipation south of the ice front is approximately 3.5×10^9 W.

outflowing layers (differences between the two layers due to meltwater is assumed negligible), W is the horizontal width of the channel (taken from observations of the width of the out-flowing DISW), L is the horizontal length of the channel (the distance between the ice front and the shallow seabed ridge southeast of Crary Ice Rise along the deep seabed channel), and $\langle k|u| \rangle$ is the friction parameter for the time independent circulation (the tidal current magnitude scales this parameter).

The density difference $\Delta\rho$ may be expressed in terms of the temperature difference $\Delta\theta$ between the inflow and the freezing temperature of the ice shelf base where melting occurs, by using the calorimetric relationship given by Griesman [1979]:

$$\Delta\rho = \beta\rho c S \Delta\theta/L_0 \tag{6}$$

where $S = 34.75$ ‰ is the salinity of the inflow, $c = 3989$ J/kg°C is the heat capacity of sea water at 0°C [Gill, 1983, p. 601], $L_0 = 3.34 \times 10^5$ J/kg is the latent heat of fusion [Wallace and Hobbs, 1977, p. xvii], and $\beta = 0.8 \times 10^{-3}$ ‰$^{-1}$.

The balance between the two mechanical energy terms defined by equations (4) and (5) may be solved for u_c:

$$u_c = (g\Delta Dh\beta c S/(LL_0 k|u|)) \Delta\theta \tag{7}$$

Appropriate values for the parameters determined from the observed hydrographic conditions off the ice front and from the basin dimensions ($\Delta\theta = 0.2°C$, $\Delta D = 100$ m, $k|u| = 0.5 \times 10^{-3}$ m/s, $h = 100$ m, and $L = 1000$ km) yield $u_c = 0.013$ m/s. This velocity scale estimate implies a ventilation time scale of approximately 5 years and is consistent with the radioactive tracer observations made at J9 [Michel et al., 1979].

The heat flux Q per unit width of the convection cell is

$$Q = h\rho\Delta\theta c \, u_c = 1 \times 10^6 \text{ W/m} \tag{8}$$

Assuming that the width W of the channel is 200 km (a plausible value based on the observed width of outflowing DISW) and the well-mixed zone is approximately 5.8×10^4 km² in area, the basal-melting rate F associated with the value of Q given by equation (8) is

$$F = QW/(\rho_i L_0 A) = 0.17 \text{ m/yr} \tag{9}$$

where $\rho_i = 917$ kg/m³ is the ice density. Equation (9) gives a melting rate that is between the 0.05 m/yr melt rate criterion determining the maximum estimated extent of well-mixed conditions (regions indicated by shading in Figure 12) and the 0.5-m/yr criterion determining the minimum estimated extent.

Clearly, considerable leeway exists in the parameter values chosen in this simple analysis; hence, the result given by equation (9) provides only a self-consistency check rather than an independent verification of the sub-ice-shelf circulation. In the future, a more detailed thermohaline circulation simulation that emphasizes rotational effects and diffusion outside of the

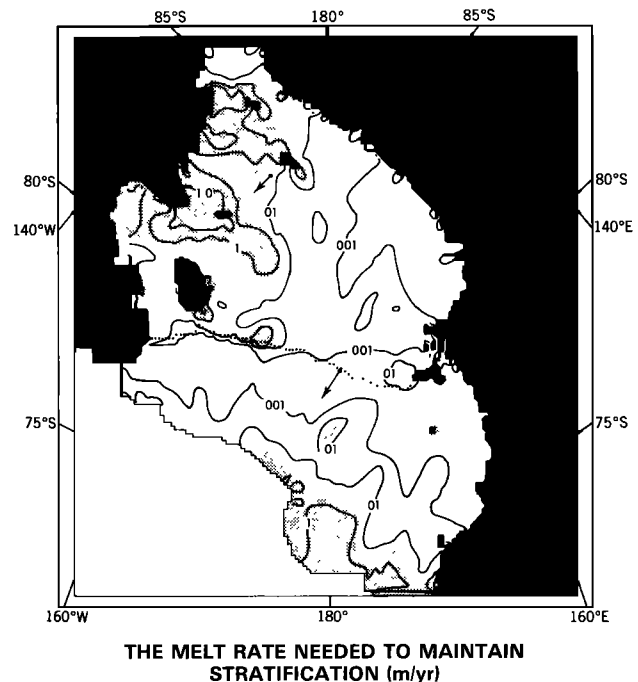**THE MELT RATE NEEDED TO MAINTAIN STRATIFICATION (m/yr)**

Fig. 12. Shaded regions indicate where tidal energy dissipation is expected to cause vertically well-mixed waters. Unshaded regions indicate where stratification characterized by warm and salty water at the seabed and cold meltwater at the ice shelf base will suppress basal melting. Contours represent the minimum basal melting rate required to stratify the water column. The 0.05 m/yr contour is expected to define the position of the tidal fronts separating vertically well-mixed waters from stratified waters. Sensitivity of this position to error of the 0.05 m/yr melt rate criterion is reduced by the steepness of the minimum melt rate gradient along the Siple Coast. The well-mixed regions predicted near the ice front and in the open part of the Ross Sea are probably incorrect because of larger basal melting rates. The vector drawn in the southeastern section represents the vertical shear of the time-average current given by the 48-hour current meter record obtained through the J9 bore hole by Jacobs (as reported in Jacobs and Haines [1982]). The lower layer moves with respect to the upper layer at a rate of 0.012 m/s in the direction indicated by the vector. This vertical shear may be explained by the slope of the isopycnal surfaces likely to be induced by the predicted tidal front southeast of J9. The vector drawn near the ice front indicates the direction of the 0.016 m/s DISW outflow determined from a 7-month current meter record [Jacobs and Haines, 1982].

well-mixed areas should be accomplished to test further the scenario proposed in this study.

Sensitivity to Climatic Change

The sub-ice-shelf thermohaline circulation model discussed above allows a preliminary assessment of the effects of climatic change on the Antarctic ice shelves. These effects could potentially have an impact on the grounded parts of the Antarctic Ice Cap because ice shelves restrain the rapid thinning that could otherwise occur in west Antarctica [Hughes, 1973]. Indeed, the present Ross and Ronne-Filchner ice shelves are largely responsible for the continued existence of the West Antarctic Ice Sheet since the last glacial maximum [Stuiver et al., 1981].

According to equations (7), (8), and (9), the basal-melting rate is proportional to $\Delta\theta^2$; thus, changing oceanic temperature will induce a nonlinear response. Doubling $\Delta\theta$ from its present value (0.2°C) to 0.4°C, for example, would increase the basal ablation rate along the Siple Coast by a factor of 4 from its present value (assumed to be 0.05 m/yr) to 0.20 m/yr.

Under present climatic conditions, HSSW is constrained to have the sea surface freezing temperature of approximately −1.9°C. This constraint therefore buffers $\Delta\theta$ from significant change and implies that the basal melting conditions are impervious to climatic change unless, of course, the change is sufficiently drastic to eliminate HSSW altogether.

One possible climatic influence of sufficient severity to upset this buffer may be the CO_2 "greenhouse" effect. Atmospheric CO_2 warming could conceivably eliminate the formation of HSSW by halting winter sea ice growth altogether or by producing a near-surface pycnocline that prevents deep convection. Wetherald and Manabe [1981] have examined the seasonal cycle of the CO_2-rich climate using an idealized global distribution of continent and ocean. Their results indicate that sea ice production is entirely eliminated throughout all four seasons in the latitude range of the Ross Sea. Another experiment by Manabe and Stouffer [1980] using more realistic global distribution of land and sea, however, mitigates this result by indicating that winter sea ice growth off Antarctica is reduced but not entirely eliminated.

The relationship between the Antarctic ice mass and global climate change resulting from atmospheric CO_2 is clearly a subject of continuing development. The results of this study indicate that the seasonal sea ice growth cycle, and the associated production of HSSW, are the most important climatic variables effecting sub-ice-shelf ocean circulation and basal melting.

Another potential change that could upset the basal-melting-rate buffer is an ice front advance out to the northern edge of the continental shelf. Although of interest primarily in paleoclimatic studies, such an advance would cause high salinity water masses formed by offshore sea ice advection to convect into the abyssal ocean directly rather than onto the shallow, confining shelves. This potential behavior suggests that ice sheet growth in west Antarctica may be self-limiting: Once the ice front advances to the continental shelf margin, strong basal melting along the grounding line is no longer prevented by HSSW. Ice front retreat away from the continental shelf margin would not necessarily follow immediately after grounding line retreat is triggered; hence, a significant lag may exist in this possible feedback mechanism.

References

Bentley, C. R., J. W. Clough, K. C. Jezek, and S. Shabtaie, Ice-thickness patterns and the dynamics of the Ross Ice Shelf, Antarctica, *J. Glaciol, 24,* 287–294, 1979.

Carmack, E. C., and T. D. Foster, Circulation and distribution of oceanographic properties near the Filchner Ice Shelf, *Deep Sea Res., 22,* 77–90, 1975.

Clough, J. W., and B. L. Hansen, The Ross Ice Shelf Project, *Science, 203,* 433–434, 1979.

Fearnhead, P. G., On the formation of fronts by tidal mixing around the British Isles, *Deep Sea Res., 22,* 311–321, 1975.

Foster, T. D., The temperature and salinity fine structure of the ocean under the Ross Ice Shelf, *J. Geophys. Res., 88,* 2556–2564, 1983.

Gammelsrod, T., and N. Slotsvik, Hydrographic and current measurements in the southern Weddell Sea 1979/80, *Polarforshung, 51,* 101–111, 1981.

Gill, A. E., Circulation and bottom water production in the Weddell Sea, *Deep Sea Res., 20,* 111–140, 1973.

Gill, A. E., *Atmosphere-Ocean Dynamics,* Academic, New York, 1982.

Gilmore, A. E., Ross Ice Shelf sea temperatures, *Science, 203,* 438–439, 1979.

Greenberg, D. A., A numerical model investigation of tidal phenomena in the Bay of Fundy and Gulf of Maine, *Mar. Geod., 2,* 161–187, 1979.

Greischar, L. L., and C. R. Bentley, Isostatic equilibrium grounding line between the West Antarctic inland ice sheet and the Ross Ice Shelf, *Nature, 283,* 651–654, 1980.

Greisman, P., On upwelling driven by the melt of ice shelves and tidewater glaciers, *Deep Sea Res., 26,* 1051–1065, 1979.

Hayes, D. E., and F. J. Davey, A geophysical study of the Ross Sea, Antarctica, in *Initial Reports of the DSDP,* vol. 28, edited by D. E. Hayes et al., pp. 263–278, Government Printing Office, Washington, D. C., 1974.

Hughes, T. J., Is the West Antarctic ice sheet disintegrating?, *J. Geophys. Res., 78,* 7884–7910, 1973.

Hughes, T. J., The West Antarctic ice sheet: Instability, disintegration, and initiation of ice ages, *Rev. Geophys. Space Phys., 13,* 502–526, 1975.

Huthnance, J. M., Large tidal currents near Bear Island and related tidal energy losses from the North Atlantic, *Deep Sea Res., 28,* 51–70, 1981.

Jacobs, S. S., and W. E. Haines, Oceanographic data in the Ross Sea and along the George V Coast, 1976–1979, *Ross Ice Shelf Proj. Tech. Rep. LDGO-82-1,* Lamont-Doherty Geol. Observatory, Palisades, New York, 1982.

Jacobs, S. S., A. F. Amos, and P. M. Bruchausen, Ross Sea oceanography and Antarctic bottom water formation, *Deep Sea Res., 17,* 935–962, 1970.

Jacobs, S. S., A. L. Gordon, and J. L. Ardai, Jr., Circulation and melting beneath the Ross Ice Shelf, *Science, 203,* 441–443, 1979.

Killworth, P. D., A baroclinic model of motions on Antarctic continental shelves, *Deep Sea Res., 21,* 815–837, 1974.

Killworth, P. O., Some models of bottom water formation, in *Polar Oceans,* edited by M. J. Dunbar, pp. 179–189, Arctic Institute of North America, Calgary, 1977.

Kowalik, Z., and N. Untersteiner, A study of the M2 tide in the Arctic Ocean, *Deut. Hydrogr. Zeit., 31,* 216–229, 1978.

Longuet-Higgins, M. S., On the trapping of waves along a discontinuity of depth in a rotating ocean, *J. Fluid Mech., 31,* 417–435, 1968.

Lusquinos, A. J., Extreme temperatures in the Weddell Sea, *Årbok Univ. Bergen, Mat. Naturvit. Ser., 23,* 1–19, 1963.

MacAyeal, D. R., Numerical simulations of the Ross Sea Tides, *J. Geophys. Res.,* in press, 1983a.

MacAyeal, D. R., Rectified tidal currents and tidal-mixing fronts: Controls on the Ross Ice Shelf flow and mass balance, Ph.D. Thesis, Princeton Univ., Princeton, N. J., 1983b.

Manabe, S., and R. J. Stouffer, Sensitivity of a global climate model to an increase of CO_2 concentration in the atmosphere, *J. Geophys.*

Res., *85*, 5529-5554, 1980.

Michel, R. L., T. W. Linick, and P. M. Williams, Tritium and carbon-14 distributions in sea water from under the Ross Ice Shelf Project ice hole, *Science*, 203, 445-446, 1979.

Miller, G. R., The flux of tidal energy out of the deep oceans, *J. Geophys. Res.*, *71*, 2485-2489, 1966.

Pingree, R. D., Physical oceanography of the Celtic Sea and English Channel, in *The Northwest European Shelf Seas: the Sea Bed and the Sea in Motion*, vol. 2, *Physical and Chemical Oceanography and Physical Resources*, edited by F. T. Banner, M. B. Collins, and K. S. Massie, pp. 415-466, Elsevier, New York, 1980.

Pingree, R. D., and D. K. Griffiths, Tidal fronts on the shelf seas around the British Isles, *J. Geophys. Res.*, *83*, 4615-4622, 1978.

Pingree, R. D., and L. Maddock, Tidal residuals in the English Channel, *J. Mar. Biol. Assoc. U. K.*, *57*, 339-354, 1977.

Ramming, H. G., and Z. Kowalik, *Numerical Modelling of Marine Hydrodynamics, Applications to Dynamic Physical Processes, Oceanogr. Ser.*, vol. 26, Elsevier/North Holland, New York, 1980.

Schumacher, J. D., T. H. Kinder, D. H. Pashinski, and R. L. Charnell, A structural front over the continental shelf of the eastern Bering Sea, *J. Phys. Oceanogr.*, *9*, 78-87, 1979.

Simpson, J. H., Density stratification and microstructure in the western Irish Sea, *Deep Sea Res.*, *18*, 309-319, 1971.

Simpson, J. H., and J. R. Hunter, Fronts in the Irish Sea, *Nature*, *250*, 404-406, 1974.

Stuiver, M., G. H. Denton, T. J. Hughes, and J. L. Fastook, History of the marine ice sheet in west Antarctica during the last glaciation: A working hypothesis, in *The Last Great Ice Sheets*, edited by G. H. Denton and T. J. Hughes, pp. 319-436, John Wiley, New York, 1981.

Thomas, R. H., and C. R. Bentley, The equilibrium state of the eastern half of the Ross Ice Shelf, *J. Glaciol.*, *20*, 509-518, 1978.

Truesdale, R. S., and T. B. Kellog, Ross Sea diatoms: Modern assemblage distributions and their relationship to ecologic, oceanographic, and sedimentary conditions, *Mar. Micropaleontol.*, *4*, 13-31, 1979.

Wallace, J. M., and P. V. Hobbs, *Atmospheric Science: An Introductory Survey*, Academic, New York, 1977.

Weiss, R. F., H. G. Ostlund, and H. Craig, Geochemical studies of the Weddell Sea, *Deep Sea Res.*, 26, 1093-1120, 1979.

Wetherald, R. T., and S. Manabe, Influence of seasonal variation upon the sensitivity of a model climate, *J. Geophys. Res.*, *86*, 1194-1204, 1981.

Williams, R. T., The ocean tide beneath the Ross Ice Shelf, Master of Science Thesis, Virginia Polytech. Inst. and State Univ., Blacksburg, Va., 1976.

Williams, R. T., and E. S. Robinson, The ocean tide in the southern Ross Sea, *J. Geophys. Res.*, *85*, 6689-6696, 1980.

Williams, R. T., and E. S. Robinson, Flexural waves in the Ross Ice Shelf, *J. Geophys. Res.*, *86*, 6643-6648, 1981.

D. R. MacAyeal, Department of the Geophysical Sciences, The University of Chicago, 5734 South Ellis Avenue, Chicago, IL 60637.